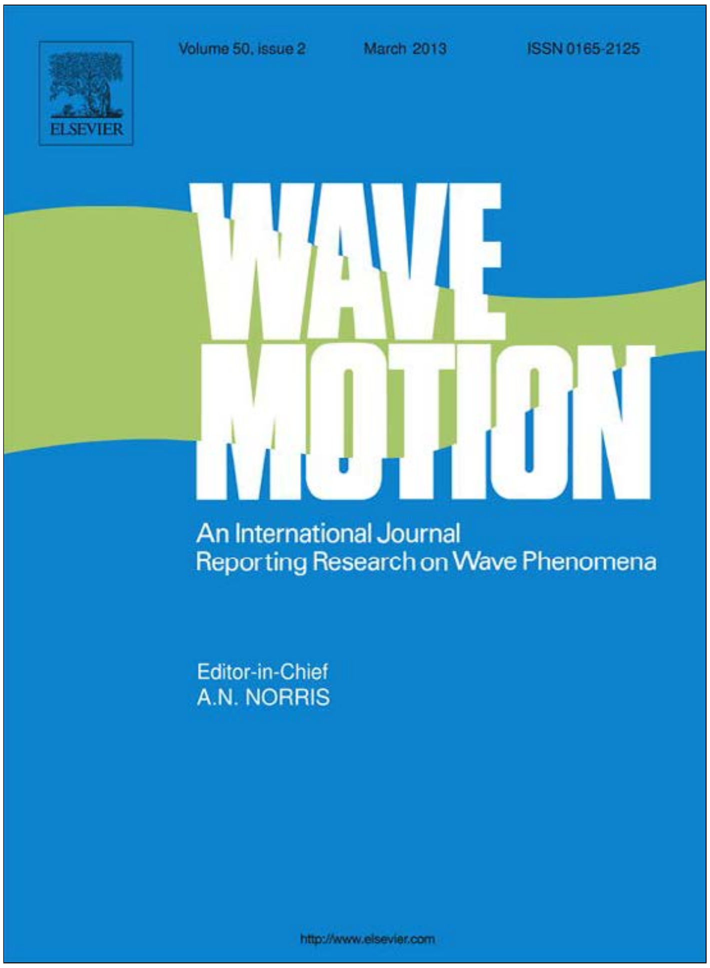
Volume 50, issue 2
March 2013
ISSN 0165-2125
ELSEVIER
WAVE MOTION
An International Journal
Reporting Research on Wave Phenomena
Editor-in-Chief
A.N. NORRIS
http://www.elsevier.com

Wave Motion 50 (2013) 310–325

Contents lists available at SciVerse ScienceDirect

Wave Motion

journal homepage: www.elsevier.com/locate/wavemoti

Simulation of flexural waves in drill pipes including the effects of the gravitational field

José M. Carcione *, Flavio Poletto, Giorgia Pinna

Istituto Nazionale di Oceanografia e di Geofisica Sperimentale (OGS), Borgo Grotta Gigante 42c, 34010 Sgonico, Trieste, Italy

ARTICLE INFO

Article history:
Received 27 February 2012
Received in revised form 22 June 2012
Accepted 11 September 2012
Available online 27 October 2012

Keywords:
Flexural waves
Simulation
Drill string
Gravitational load
Reciprocity
Neutral point

ABSTRACT

We design a full-wave modeling method to simulate flexural (bending) waves in pipes of variable cross-section and material properties, subject to the effects of the gravitational field. The study finds application in propagation through drill strings and stability of hydrocarbon wells while drilling. The algorithm is based on a direct (grid) method, where the spatial derivatives are computed with the Fourier pseudospectral method. The modeling is successfully tested against the analytical solution for flexural waves propagating in a uniform pipe. Moreover, we obtain reciprocity relations for the lateral deflection, particle velocity and bending moment due to sources applied in the force-balance and constitutive equations. The relations are then verified by the simulations and at the same time provide a test of the consistency of the numerical algorithm in inhomogeneous media, where there is no closed-form analytical solution.

We analyze the effects of the gravitational field and show that for negative axial loads (compressive stresses) there is an instability below a critical wavenumber, while the system is stable for positive (tensile) loads. Such a situation appears below the neutral point of a drill string when the gravitational force is taken into account. A plane-wave analysis yields the phase and group velocities when the load is uniform along the pipe and in the case of a suspended pipe subject to a gravitational force with a neutral point downhole. In the latter case, the signal propagates with attenuation. Propagation along a realistic drill string, simulating the drill bit as a stress-free end, is illustrated. Moreover, propagation subject to an axial gravitational load shows that the signal is slower for a tensile prestress.

1. Introduction

Wellbore stability is essential in drilling operations. One of the features generating instabilities are flexural waves – also termed bending, lateral and transverse waves – propagating through the drill string. This system consists of a series of hollow cylindrical steel pipes to which is attached a short heavier segment, the bottom-hole assembly (BHA), including at its end a cutting device (the drill-bit). The assembly is driven in a rotary fashion, and typically axial, torsional and flexural (bending or lateral) waves are generated through the drill string. Bending motions are produced by pipe–borehole contacts, bit whirling and stick slip and may cause the failure of the BHA in exploration and production wells [1,2]. It is therefore important to correctly model flexural motions in an assembly of drill pipes when sources and receivers are used for communication and vibration analysis, to monitor the conditions of the drill string and obtain information about the geological formations [3].

Flexural waves are one of the causes generating instabilities in pipes, rods and beams [4–6]. In particular, this may happen when the pipe is subject to a prestress axial load. It is the case of drill strings, wherein the gravitational stiffening effect and the weight-on-bit divides the hanging string into two sections, namely, an upper tensile part and a lower compressive

* Corresponding author. Tel.: +39 040 2140345; fax: +39 040 327521.
E-mail address: jcarcione@inogs.it (J.M. Carcione).

0165-2125/$ – see front matter
doi:10.1016/j.wavemoti.2012.09.003

part, separated by the so-called neutral point. Buoyancy effects due to the presence of mud can easily be included in the model.

The equations of motion for flexural waves, including the effect of prestress, are based on the Bernoulli–Euler beam theory [4] for which some reciprocity relations have already been established [7]. We assume the thin-rod approximation, which holds for wavelengths much larger than the radial dimensions of the pipes, neglect mode conversions, the effects of drill string rotation, the presence of the drilling mud and the interaction with the borehole walls, unless for the presence of bending sources located at different points of the assembly. Mainly, the effects of the wall contact and of the drilling mud is to damp the bending motions [8]. Mud flow-induced forces are neglected since we consider a vertical straight borehole and its effects are of second order. Due to the same reason, wall contacts and mode conversions are neglected. Although these factors can be relatively important in some cases, the main scope here is to study the effects of the gravitational field. See Shyu [9], Gulyaev et al. [10] and Sahebkar et al. [11] for the effects of drill-string wall interactions and inclined boreholes. Graff [4] gives the dispersion relation and shows that an instability occurs for finite beams if the axial load is compressive. We obtain the phase and group velocities of the flexural waves as a function of the axial load and show that a similar instability is present in unbounded beams under compressive stresses. We also obtain reciprocity relations for the deflection field, and test these relations by using a full-wave solver based on a direct grid method [12].

Then, we simulate flexural motions in a vertical drill string composed of pipes of different dimensions, and study the effects of a constant axial load and a linearly varying axial load due to gravity. The algorithm to simulate flexural vibrations is based on a 4th-order Runge–Kutta technique as time-stepping algorithm, and the Fourier method to compute the spatial derivatives by means of the Fast Fourier Transform (FFT) [13]. This approximation is infinitely accurate for band-limited periodic functions with cutoff spatial wavenumbers which are smaller than the cutoff wavenumbers of the mesh.

2. Equation of motion

Flexural waves in pipes subject to prestress are governed by the following equation of motion [4]

$$\begin{aligned} &\eta \ddot{w} = M_{,zz} + (T w_{,z})_{,z} + s, \quad \eta = \rho A, \\ &\gamma^{-1} M = w_{,zz} + m, \quad \gamma = -EI, \end{aligned} \tag{1}$$

where $w(z)$ is the deflection, $M(z)$ is the bending moment, $T(z)$ is the prestress or axial load, $\rho(z)$ is the mass density, $A(z) = \pi(r_o^2 - r_i^2)$ is the area of the pipe, r_i and r_o are the inner and outer radii of the pipe, respectively, E is Young's modulus,

$$I = \frac{\pi}{4}(r_o^4 - r_i^4), \tag{2}$$

is the transverse moment of inertia, s is a force per unit length and m is an external moment source. A dot above a variable denotes time differentiation and a subscript ",z" indicate spatial derivatives with respect to the variable z. The first equation (1) is Newton–Euler law (balance of forces) and the second one is the constitutive equation.

Eq. (1) is used to model flexural waves in drill strings with variable properties. It is well known that the dispersion relation related to Eq. (1) has four solutions [4,5,12]. The first two roots correspond to progressive and regressive waves (far-field modes), while the others are static modes. One root is an unstable diverging mode, and the other corresponds to energy stored in stable local resonances, i.e., near-field effects [3,14].

3. Plane-wave analysis and instability

3.1. Constant axial load

Assuming a uniform axial load and eliminating the bending moment in Eq. (1), we obtain

$$a^{-2}\ddot{w} + w_{,zzzz} - 2\zeta w_{,zz} = 0, \tag{3}$$

where

$$a = \sqrt{\frac{EI}{\rho A}} \quad \text{and} \quad \zeta = \frac{T}{2EI}, \tag{4}$$

and we have assumed a homogeneous medium and $s = m = 0$.

Let us consider the plane-wave kernel $\exp(\mathrm{i}\omega t - \mathrm{i}kz)$, where $\mathrm{i} = \sqrt{-1}$, ω is the angular frequency and k is the wavenumber. Substituting this expression into Eq. (3) gives the dispersion relation [4]

$$k^4 + 2\zeta k^2 - a^{-2}\omega^2 = 0. \tag{5}$$

We obtain from (5):

$$\omega = \pm ak\sqrt{k^2 + 2\zeta}. \tag{6}$$

The system is stable if ω is a real root of Eq. (5) for all k's. Conversely, it is unstable if there is, at least, one value of k for which the root ω becomes imaginary. In the latter case, the solution grows exponentially in time, since a normal-mode solution of the form $\exp(|\omega|t)$ develops. If $T > 0$ there is no instability, while $T < 0$, i.e. a compressive load, implies that the system is unstable for

$$k < k_{\mathrm{cr}} = \sqrt{2|\zeta|} = \sqrt{\frac{|T|}{EI}}, \tag{7}$$

where k_{cr} is a critical wavenumber. If $k \ll k_{\mathrm{cr}}$, the pipe behaves like a tension-free beam, while for $k \gg k_{\mathrm{cr}}$ it behaves like a string. Instability due to buckling occurs when the two ends of the pipes are fixed and also when there is interaction with torsional waves [3]. A playing card under compression or mountain folding is described by the same theory [4,15].

Let us consider $E = 206$ GPa, $\rho = 7850$ kg/m^3 (steel), and the drill pipe radii: $r_i = 5.44$ cm and $r_o = 6.35$ cm. Using Eq. (2) we have $EI = 1.21$ MN. Consider a compressive load $T = -\rho gAL$, where $gr = 9.81$ m/s^2 is the acceleration of gravity and $L = 200$ m of drill pipe below the neutral point (see below, Eq. (16)). It yields $T = -52$ kN, $\zeta = 0.021$ m^{-2} and $k_{\mathrm{cr}} = 0.2$ m^{-1}. This means that if the signal has wavenumbers smaller than k_{cr}, the system will be unstable.

We can verify if instability occurs for a given frequency $f = \omega/(2\pi)$ by calculating the minimum wavenumber of the propagating modes. The roots of Eq. (5) are

$$k = \pm\sqrt{-\zeta \pm \sqrt{\zeta^2 + \omega^2/a^2}}. \tag{8}$$

If $T > 0$ or $\zeta > 0$ (tension) the wavenumbers are

$$\pm\,\alpha, \qquad \pm\mathrm{i}\beta, \tag{9}$$

where

$$\alpha = \sqrt{-|\zeta| + \sqrt{\zeta^2 + \omega^2/a^2}}, \qquad \beta = \sqrt{|\zeta| + \sqrt{\zeta^2 + \omega^2/a^2}}. \tag{10}$$

If $T < 0$ or $\zeta < 0$ (compression) the wavenumbers are

$$\pm\,\beta, \qquad \pm\mathrm{i}\alpha. \tag{11}$$

The first two roots correspond to progressive and regressive waves, while the others are static modes. One root is an unstable diverging mode, and the others correspond to energy stored in stable local resonances, i.e., near-field effects [3,14]. Then, from Eq. (6), frequencies satisfying

$$f < \frac{a\beta}{2\pi}\sqrt{\beta^2 - 2|\zeta|} \tag{12}$$

are within the unstable range.

The phase velocity of the wave modes is given by

$$\begin{aligned} v_p &= \omega/\alpha, \quad \text{tensile load}, \\ v_p &= \omega/\beta, \quad \text{compressive load}. \end{aligned} \tag{13}$$

On the other hand, the group velocity is, from (5),

$$v_g = \frac{\partial\omega}{\partial k} = \partial_k\omega = \frac{2a^2k}{\omega}(k^2 + \zeta). \tag{14}$$

Then,

$$\begin{aligned} v_g &= 2a^2\alpha\omega^{-1}(\alpha^2 + \zeta), \quad \text{tensile load}, \\ v_g &= 2a^2\beta\omega^{-1}(\beta^2 + \zeta), \quad \text{compressive load}. \end{aligned} \tag{15}$$

Let us assume $f = 30$ Hz and $|T| = 52$ kN. We obtain $v_p(\text{tensile}) = 204$ m/s, $v_p(\text{compressive}) = 198$ m/s, $v_g(\text{tensile}) = 387$ m/s and $v_g(\text{compressive}) = 417$ m/s. As can be seen, although pre-compression implies a smaller phase velocity [4], the group velocity is higher than that of pre-tension.

3.2. Axial load due to the gravitational field

The axial load due to gravity has the expression

$$T = \rho A g (z - z_n), \tag{16}$$

where z_n is the neutral point. The z-axis points upwards and $z = 0$ is located below the neutral point (e.g., the drill bit). We re-write (16) as

$$\frac{T}{EI} = 2\zeta + \xi z, \tag{17}$$

where

$$\zeta = -\frac{\rho A g z_n}{2EI} \quad \text{and} \quad \xi = \frac{\rho A g}{EI}. \tag{18}$$

Assuming a uniform axial load and eliminating the bending moment in Eq. (1), we obtain

$$a^{-2}\ddot{w} + w_{,zzzz} - \xi w_{,z} - \xi z w_{,zz} - 2\zeta w_{,zz} = 0. \tag{19}$$

Substituting the plane-wave kernel $\exp(\mathrm{i}\omega t - \mathrm{i}kz)$ yields

$$k^4 + \left(\frac{T}{EI}\right) k^2 + \mathrm{i}\xi k - a^{-2}\omega^2 = 0, \tag{20}$$

where we have used Eq. (17). Note that $T = T(z)$. Eq. (20) is a generalization of Eq. (5). It is a quartic which has four complex roots, and therefore the propagation modes have dissipation. Let k be a root. We define the complex velocity as

$$v = \frac{\omega}{k}. \tag{21}$$

Then, the phase velocity and attenuation factor are obtained from the complex velocity as [13]

$$v_p = \left[\mathrm{Re}\left(v^{-1}\right)\right]^{-1} \quad \text{and} \quad \alpha = -\omega \mathrm{Im}(v^{-1}), \tag{22}$$

respectively.

The group velocity is $\partial_\kappa \omega$, where $\kappa = \mathrm{Re}(k)$ is the real wavenumber. Then

$$v_g = (\partial_\omega \kappa)^{-1} = [\partial_\omega \mathrm{Re}(k)]^{-1} = [\mathrm{Re}(\partial_k \omega)]^{-1}. \tag{23}$$

The quantity $\partial_k \omega$ can easily be obtained from (20). We get

$$\partial_k \omega = \frac{a^2}{2\omega}\left[4k^3 + 2\left(\frac{T}{EI}\right)k + \mathrm{i}\xi\right]. \tag{24}$$

4. Reciprocity relations

The reciprocity principle is established by considering two experiments, denoted by superscripts A and B, and combining the two Eqs. (1) into one as

$$\begin{aligned} \eta \ddot{w}^A &= (\gamma w^A_{,zz})_{,zz} + (T w^A_{,z})_{,z} + \gamma m^A_{,zz} + s^A, \\ \eta \ddot{w}^B &= (\gamma w^B_{,zz})_{,zz} + (T w^B_{,z})_{,z} + \gamma m^B_{,zz} + s^B. \end{aligned} \tag{25}$$

Multiplying the first equation by w^B and the second by w^A and subtracting yields

$$\begin{aligned} &(\eta \ddot{w}^A - \gamma m^A_{,zz} - s^A) w^B - (\gamma w^A_{,zz})_{,zz} w^B - (\eta \ddot{w}^B - \gamma m^B_{,zz} - s^B) w^A + (\gamma w^B_{,zz})_{,zz} w^A \\ &\quad - (T w^A_{,z})_{,z} w^B + (T w^B_{,z})_{,z} w^A = 0. \end{aligned} \tag{26}$$

Now, let us integrate this equation between the two limits $z = a$ and $z = b$ and consider the second term

$$I^{AB} = \int_a^b (\gamma w^A_{,zz})_{,zz} w^B dz = \int_a^b w^B d(\gamma w^A_{,zz})_{,z} = \left| w^B (\gamma w^A_{,zz})_{,z} \right|_a^b - J^{AB}, \tag{27}$$

where we have integrated by parts, and J^{AB} is given by

$$J^{AB} = \int_a^b w^B_{,z}\, d(\gamma w^A_{,zz}) = \left| w^B_{,z} \gamma w^A_{,zz} \right|_a^b - \int_a^b \gamma w^A_{,zz} w^B_{,zz} dz, \tag{28}$$

after a new integration by parts. Hence,

$$I^{AB} = \left| w^B (\gamma w^A_{,zz})_{,z} - \gamma w^B_{,z} w^A_{,zz} \right|_a^b + \int_a^b \gamma w^A_{,zz} w^B_{,zz} dz. \tag{29}$$

Likewise, the fourth term in Eq. (26) is

$$I^{BA} = \left| w^A (\gamma w^B_{,zz})_{,z} - \gamma w^A_{,z} w^B_{,zz} \right|_a^b + \int_a^b \gamma w^A_{,zz} w^B_{,zz} dz. \tag{30}$$

On the other hand, using the integration by parts,

$$\int_a^b \left[(T w^A_{,z})_{,z} w^B - (T w^B_{,z})_{,z} w^A \right] dz = \left| w^B T w^A_{,z} - w^A T w^B_{,z} \right|_a^b . \tag{31}$$

Integrating and replacing these results into Eq. (26) yield

$$\begin{aligned} &\int_a^b [(\eta \ddot{w}^A - \gamma m^A_{,zz} - s^A) w^B - (\eta \ddot{w}^B - \gamma m^B_{,zz} - s^B) w^A] dz \\ &\quad = \left| -(\gamma w^B_{,zz})_{,z} w^A + \gamma w^B_{,zz} w^A_{,z} + (\gamma w^A_{,zz})_{,z} w^B - \gamma w^A_{,zz} w^B_{,z} + w^B T w^A_{,z} - w^A T w^B_{,z} \right|_a^b . \end{aligned} \tag{32}$$

Performing a time-Fourier transform, time derivatives can be replaced by iω. It yields

$$\begin{aligned} &\int_a^b [(s^B + \gamma m^B_{,zz}) w^A - (s^A + \gamma m^A_{,zz}) w^B] dz \\ &\quad = \left| -(\gamma w^B_{,zz})_{,z} w^A + \gamma w^B_{,zz} w^A_{,z} + (\gamma w^A_{,zz})_{,z} w^B - \gamma w^A_{,zz} w^B_{,z} + w^B T w^A_{,z} - w^A T w^B_{,z} \right|_a^b . \end{aligned} \tag{33}$$

The right side in this equation vanishes if the limits a and b are taken at the far field, where the static modes are attenuated. In this case, the situation is similar to that of the reciprocity principle for the acoustic wave equation, where the limiting absorption condition is used. We obtain

$$\int_a^b [(s^B + \gamma m^B_{,zz}) w^A - (s^A + \gamma m^A_{,zz}) w^B] dz = 0. \tag{34}$$

We consider forces and moments whose spatial functions are Dirac's delta centered at z_A and z_B in experiments A and B, respectively, and whose time history is $h(t)$, e.g.,

$$s^A(t, z) \propto \delta(z - z_A) h(t). \tag{35}$$

Omitting for simplicity the time history, the following reciprocal experiments can be identified:

$$\begin{aligned} &s^A = \delta(z - z_A) \quad \text{and} \quad s^B = \delta(z - z_B) \to w^A(z_B) = w^B(z_A), \\ &m^A = \delta(z - z_A) \quad \text{and} \quad m^B = \delta(z - z_B) \to \gamma(z_B) w^A_{,zz}(z_B) = \gamma(z_A) w^B_{,zz}(z_A). \end{aligned} \tag{36}$$

When we apply f, $m = 0$ and vice versa.

4.1. Reciprocity of the bending moment

The reciprocity principle for the moment field is obtained by eliminating the deflection in Eqs. (1). By exploiting the symmetry of these equations, we can use the same mathematical procedure applied above if we identify $w \to M$ and $\eta \to \gamma^{-1}$ and take into account that the source is $\ddot{g}$ rather than g in the equation of motion of the bending moment. We then obtain the following reciprocal experiments:

$$\begin{aligned} &s^A = \delta(z - z_A) \quad \text{and} \quad s^B = \delta(z - z_B) \to \eta^{-1}(z_B) M^A_{,zz}(z_B) = \eta^{-1}(z_A) M^B_{,zz}(z_A), \\ &m^A = \delta(z - z_A) \quad \text{and} \quad m^B = \delta(z - z_B) \to M^A(z_B) = M^B(z_A). \end{aligned} \tag{37}$$

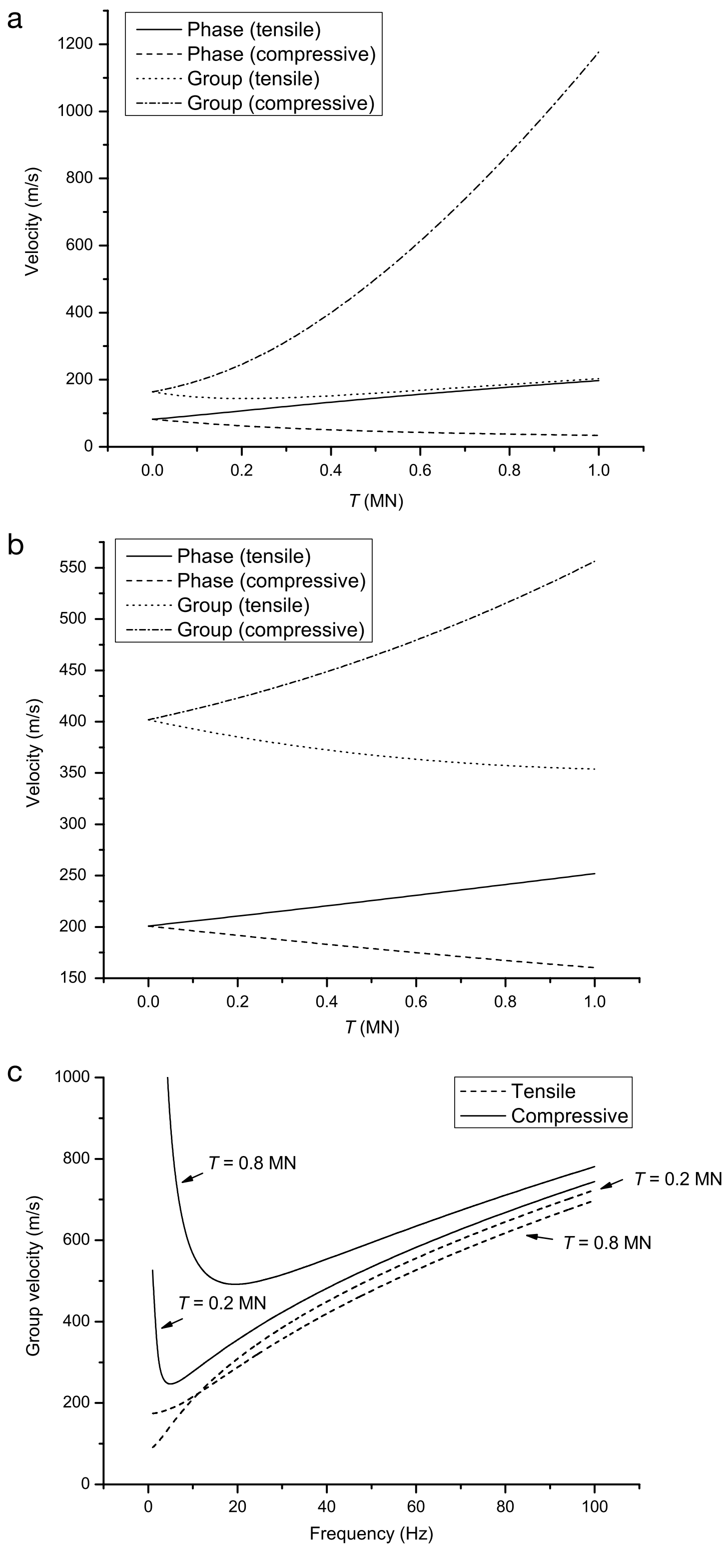

Fig. 1. Phase and group velocities as a function of tensile and compressive axial loads corresponding to $f = 5$ Hz (a) and $f = 30$ Hz (b), and group velocities versus frequency for two values of the load (c).

5. Numerical modeling

In order to obtain the equation of motion for the numerical simulation algorithm, we recast Eqs. (1) in the particle-velocity formulation. Let us introduce the gravity force

$$F = -Tw_{,z}, \tag{38}$$

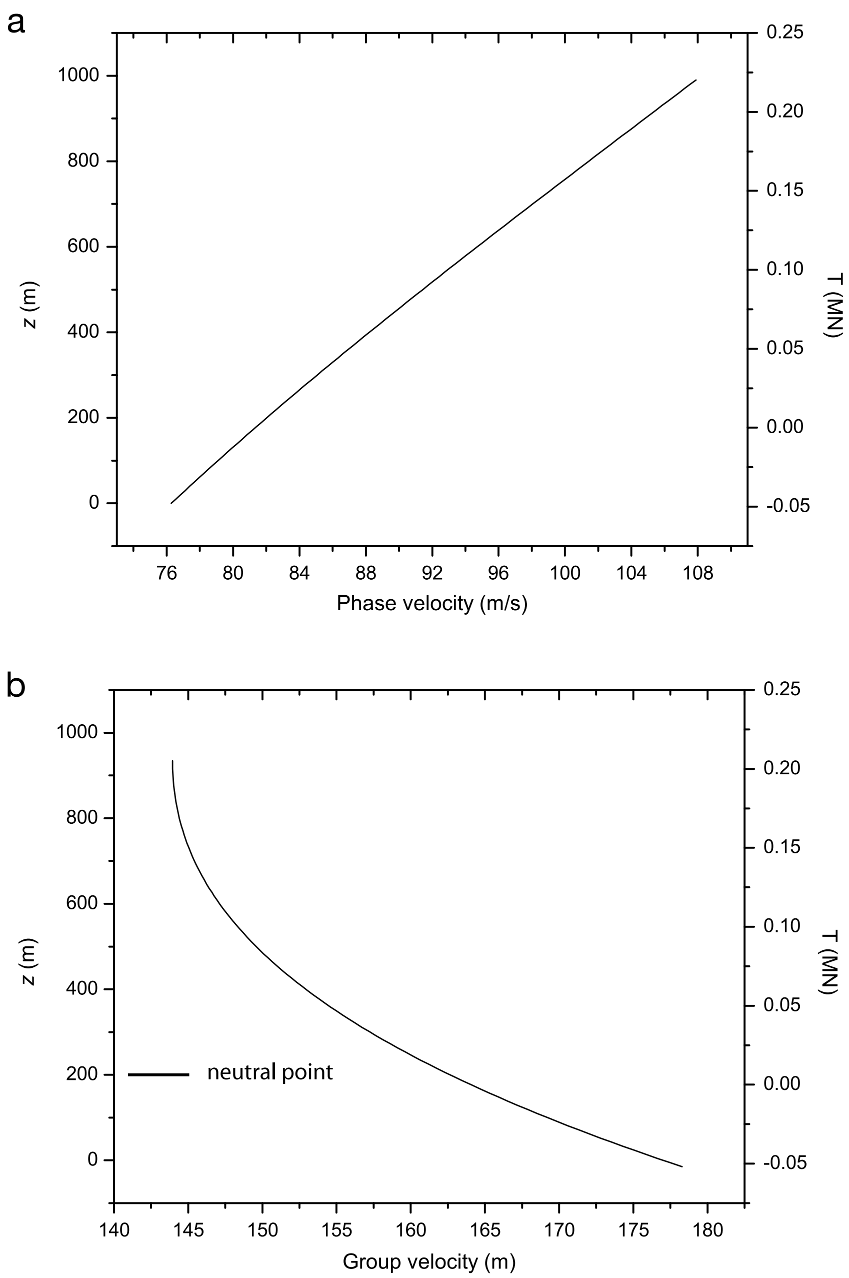

Fig. 2. Phase (a) and group (b) velocities as a function of depth and the axial gravity load. The neutral point is located at 200 m. Below this point the load is compressive. The frequency is 5 Hz.

where T can be constant or linearly varying with z as in Eq. (16). Defining $v = \dot{w}$, we obtain

$$\begin{aligned} \eta\dot{v} &= M_{,zz} - F_{,z} + s, \\ \gamma^{-1}\dot{M} &= v_{,zz} + \dot{m}, \\ \dot{F} &= -Tv_{,z}. \end{aligned} \tag{39}$$

This system can be written in the vector form as

$$\dot{\mathbf{v}} = \mathbf{H}\mathbf{v} + \mathbf{s}, \tag{40}$$

where $\mathbf{v} = (v, M, F)^\top$ is the field vector, $\mathbf{s} = (\eta^{-1}s, \gamma\dot{m}, 0)^\top$ is the source vector, and

$$\mathbf{H} = \begin{pmatrix} 0 & \eta^{-1}\partial^2_{zz} & -\partial_z \\ \gamma\partial^2_{zz} & 0 & 0 \\ -T\partial_z & 0 & 0 \end{pmatrix} \tag{41}$$

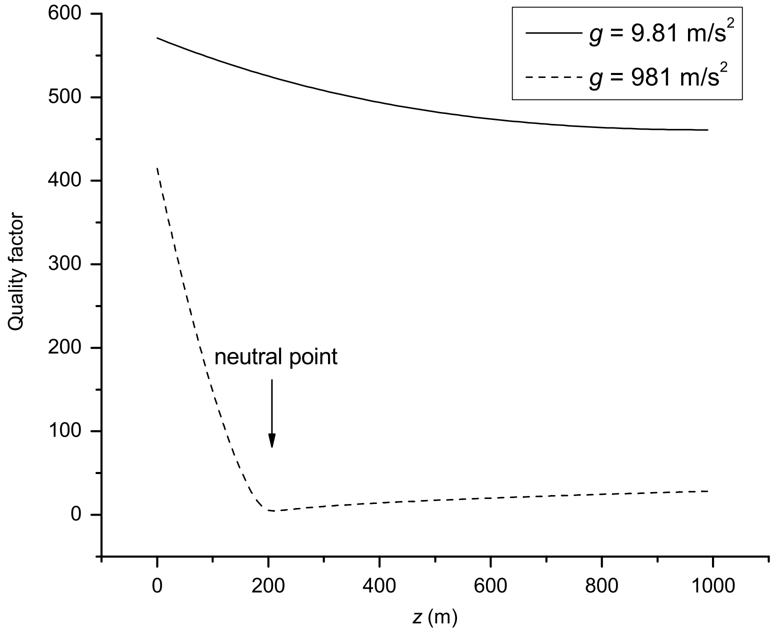

Fig. 3. Quality factor as a function of depth for two values of the gravitational constant. The neutral point is indicated. The frequency is 5 Hz.

is the propagation matrix, with ∂_z indicating a spatial derivative. The evolution Eq. (40) is solved by using a Runge–Kutta method for time integration and the Fourier pseudospectral method to compute the spatial derivatives [13]. The direct or heterogeneous formulation implicitly incorporates the boundary conditions by constructing discrete representations using the equation of motion for heterogeneous media. The spatial solver has been used to solve the one-dimensional telegraph equation for electric drill-string telemetry [16]. The algorithm requires a spatial discretization. At the top of the drill string, absorbing boundary conditions based on the sponge method are used [13], while at the bottom the stress-free end (the drill bit) is simulated by extending the drill collar (DC) with a (fictitious) pipe of negligible cross-section. It has been found that the DC to fictitious-pipe area ratio has to be greater than 100 and less than 600 for codes written in single precision arithmetics.

In a simulation with a grid spacing dx, the wavenumbers of the Fourier pseudospectral method span from 0 to the Nyquist wavenumber, π/dx. If the source has wavenumber components below the critical one k_{cr} (see Eq. (7)), the system will be unstable.

6. Physics and simulations

We first compute the phase and group velocities as a function of the tensile and compressive axial loads and frequency (Eqs. (13) and (15)). The calculations, at two different frequencies, correspond to the drill pipe whose properties are defined in a previous section (see Fig. 1(a) and (b)). The plots at 30 Hz indicate that the phase velocity for a tensile (compressive) stress increases (decreases) with increasing axial load, while the opposite behavior occurs for the group velocities. Fig. 1(c) shows the group velocities as a function of frequency for two values of the load. At low values, the tensile and compressive velocities approach each other, while at high values they diverge. At $\omega \to 0$, we have $\alpha \to 0$ and $\beta \to \sqrt{2|\zeta|}$. In this limit, the tensile group velocity is zero and the group velocity for finite compressive loads tends to infinite. At $T = 0$ we obtain $v_g = 2v_p$, as expected.

Let us consider the effects of the gravity load. Fig. 2 shows the phase and group velocities when the neutral point is located at $z = z_N = 200$ m and $f = 5$ Hz. The calculations correspond to the drill pipe. We do not observe the remarkable decrease in the group velocity reported by Chin [5, see his Fig. 6-1]. Instead, the group velocity decreases smoothly when passing from a compressive to a tensile load through the neutral point. On the other hand, the phase velocity decreases. These plots are in agreement with those of Fig. 1. The attenuation factor is small and the associated quality factor is [13]

$$Q = \frac{\mathrm{Re}(v^2)}{\mathrm{Im}(v^2)} \approx \frac{\omega}{2v_p\alpha}.$$

Fig. 3 displays the quality factor as a function of depth for two values of g and a frequency of 5 Hz. The attenuation of the propagating bending modes is higher in a more massive planet (higher g), showing a maximum at the neutral point. The pipe section subject to a compressive load ($z < 200$ m) has less attenuation. At 30 Hz the quality factor is much higher and the propagation is practically lossless. Note that $g = 981$ m/s^2 would correspond to stresses greater than nearly 1.4 GPa for a 200 m long drill pipe, while the yield stress of steel is less than 1 GPa, so the broken curve in Fig. 3 is an approximation.

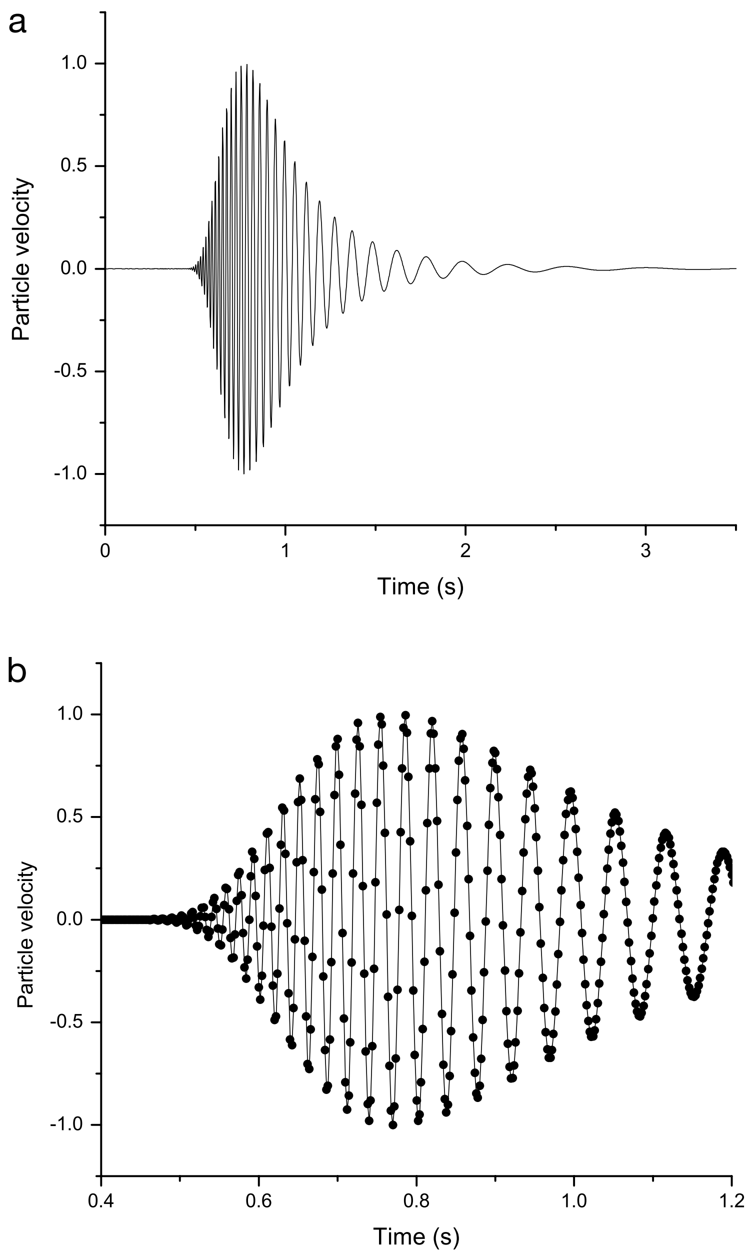

Fig. 4. Comparison between the numerical and analytical solutions corresponding to a uniform pipe. The agreement is very good (a). A detail is shown in (b), where the solid line and dots correspond to the analytical and numerical solutions (normalized field).

In order to compute the transient responses, we use a source time history of the form:

$$h(t) = \left(o - \frac{1}{2}\right) \exp(-o), \quad o = \left[\frac{\pi(t - t_s)}{t_p}\right]^2, \tag{42}$$

where t_p is the period of the wave and we take $t_s = 1.4t_p$. Its frequency spectrum is a Gaussian with a peak frequency $f_p = 1/t_p$.

We test the modeling algorithm by comparison between the analytical and numerical solutions for an unstressed uniform pipe. The Green function and the corresponding solution are given in the Appendix. Let us consider $Y = 206$ GPa, $\rho = 7850$ kg/m^3 and the drill pipe radii: $r_i = 5.44$ cm and $r_o = 6.35$ cm. Let us take $f_p = 30$ Hz, a mesh with 3465 grid points and a grid spacing of 1 m. The source is located at the grid point 1432 and the receiver at the grid point 1732, i.e., the source–receiver distance is 300 m. The algorithm requires a time step of 0.5 ms. Fig. 4 shows the comparison, where it can be seen that the agreement is excellent.

Then, we verify the reciprocity principle, which constitutes a confirmation of the consistency of the modeling method. Let us consider a section of drill string as shown in Fig. 5, where DP denotes the drill pipe, HWDP refers to the heavy-weight drill

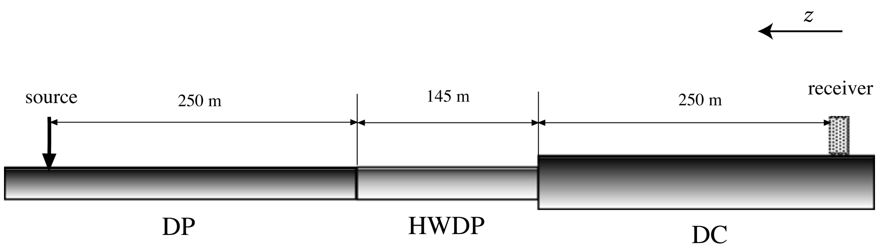

Fig. 5. Piece of drill string showing the main components: the drill pipe (DP), the heavy-weight drill pipe (HWDP) and the drill collar (DC). The receiver and source locations for a reciprocal experiment *A* are shown.

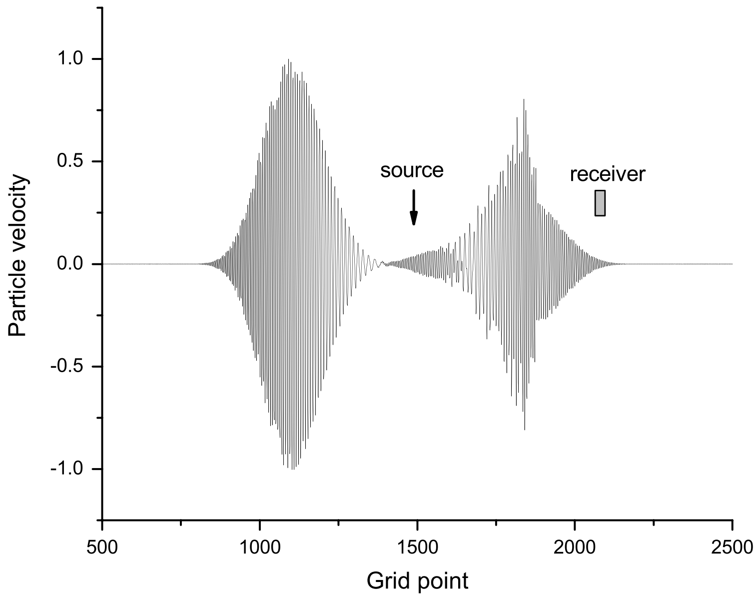

Fig. 6. Snapshot of the particle velocity at 1 s propagation, corresponding to experiment *A* shown in Fig. 5.

pipe, with $r_i = 3.81$ cm and $r_o = 6.35$ cm, and DC denotes the drill collar, with $r_i = 3.57$ cm and $r_o = 10.16$ cm. The model is not representative of a full-scale drill-string system, but of an assembly of pipe tubulars made of drill-string elements, where the locations of sources and receivers are chosen to better illustrate the reciprocity effects. The simulation has a mesh with 3465 grid points, a grid spacing of 1 m and a source central frequency $f_p = 30$ Hz. The gravity force (16) is applied, with z_N located 1338 m to the right of the receiver indicated in Fig. 5, which means that the string is in tension everywhere ($z = 0$ at grid point 3465). The algorithm requires a time step of 0.5 ms. A snapshot at 1 s propagation time is displayed in Fig. 6, where it can be seen that the bending waves are reaching the receiver. Snapshots are very useful to interpret the nature of the propagation. Fig. 7 shows the comparison between the results of experiments *A* and *B*, corresponding to the first choice of sources in Eq. (36). The agreement is excellent, confirming the reciprocity relations and the reliable performance of the modeling algorithm in the presence of pipes of different cross sections.

Considering the unstressed case, Fig. 8 shows the comparison between the results of experiments *A* and *B*, corresponding to the second choice of sources in Eq. (36), while Fig. 9 shows the comparison related to the first set of reciprocal experiments given in Eq. (37), where we consider the bending moment instead of the particle velocity. Again, the agreements are excellent.

The next simulation considers the unstressed case and experiment shown in Fig. 10, where the particle velocity is measured at receivers R1 and R2 due to a force applied at the top of the drill collar. The fictitious pipe below the drill bit has a small cross section, i.e., $r_i = 10.16$ cm and $r_o = 10.159$ cm, in order to simulate a free end (the DC to thin-pipe area ratio is approximately 500). A snapshot at 1 s propagation time is displayed in Fig. 11, where it can be seen that the bending waves have been reflected at the drill bit but have not reached the receiver (R1) located at the drill pipe. Fig. 12 shows the time responses, where the field has been normalized with respect to maximum amplitude recorded at R1.

In order to show the differences between the responses with and without the axial load, we consider a section of uniform section (DP) and the model and experiment displayed in Fig. 5. The comparison is shown in Fig. 13, where the dotted line corresponds to the absence of load. According to Eqs. (20)–(24), the group velocity in the absence of gravity ($T = 0$ and $\xi = 0$) is [4]

$$v_g = 2\sqrt{a\omega},$$

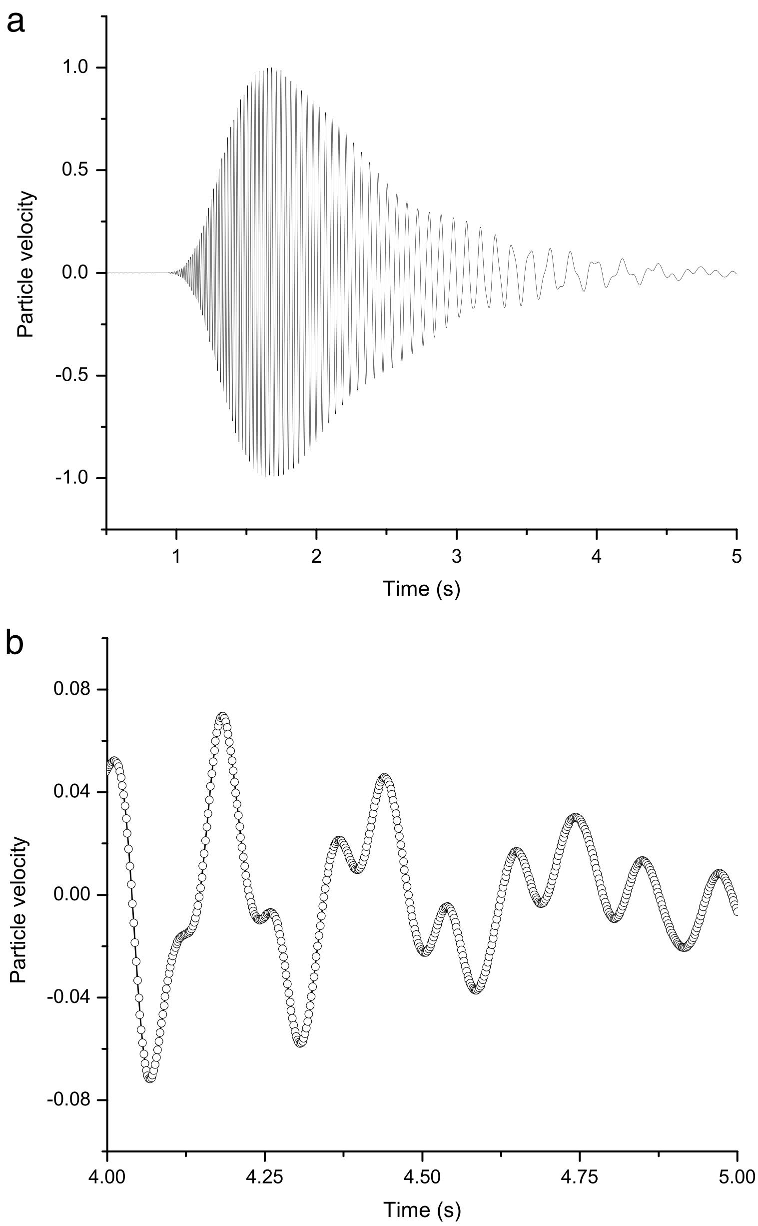

Fig. 7. Test of the reciprocity principle for the configuration shown in Fig. 5. Panel (a) shows experiments *A* and *B* (superimposed and normalized) corresponding to the first choice of sources in Eq. (36). A detail is shown in (b), where the solid line and empty dots correspond to experiments *A* and *B*, respectively.

which for 30 Hz and the drill pipe is $v_g = 401$ m/s. The group velocity for the drill pipe with an axial load of 1 MN is $v_g = 354$ m/s, according to the first equation (15). Hence, the signal is faster in the first case as it is confirmed by Fig. 13.

Finally, we show the effects of a compressible load on the time response. Let us assume that the neutral point is located at 200 m of the end of the drill collar. The neutral point location is then 938 m at the right of the receiver shown in Fig. 5. This means that the last 400 m are subject to a compressive force ($T < 0$). Fig. 14 displays the particle velocity as a function of time. As can be seen, an instability develops at 6 s propagation because wavenumbers smaller than the critical wavenumber yield imaginary frequencies (see Eq. (7)).

7. Conclusions

We have developed an algorithm to simulate flexural waves in rods and pipes based on the Bernoulli–Euler beam theory, including the effects of uniform and non-uniform axial loads, such as the gravitational force. The technique, which can handle variations in the cross sections and elastic properties of the pipes, it is based on the Runge–Kutta time-integration solver and the Fourier pseudospectral method to compute the spatial derivatives. The output can be time histories and snapshots of the deflection, particle velocity and bending moment. A plane-wave analysis indicates that the group velocity decreases or it is approximately constant with increasing axial tensile load, depending on the frequency of the signal. Instead, the group

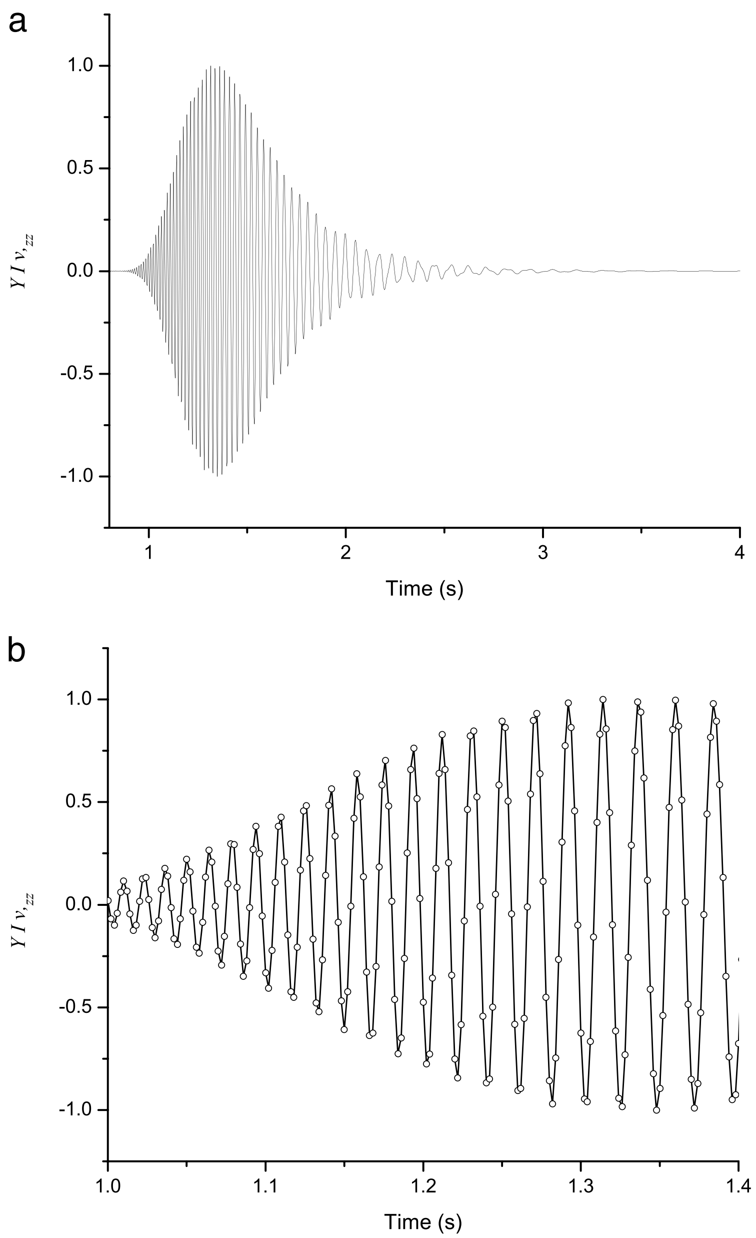

Fig. 8. Test of the reciprocity principle for the configuration shown in Fig. 5. Panel (a) shows experiments *A* and *B* (superimposed and normalized) corresponding to the second choice of sources in Eq. (36). A detail is shown in (b), where the solid line and empty dots correspond to experiments *A* and *B*, respectively.

velocity increases with increasing compressive prestress. In the case of a pipe subject to the gravitational load, this behavior implies that the velocity varies smoothly from top to bottom, when passing through the neutral point. The numerical solution has been tested with an analytical solution and reciprocal experiments. The numerical simulations verify the behavior predicted by the plane-wave analysis. A simulation illustrates how the algorithm can handle propagation through a realistic drill string. Finally, as predicted by the dispersion relation, instabilities appear under compressive loads.

Acknowledgment

We thank Fabio Cavallini for useful comments.

Appendix. The Green function in uniform media

For completeness, we report the Green function for flexural waves propagating in a uniform pipe. It is given by

$$G(z,t) = \frac{z}{4\gamma}\left[S_2[(2\pi\alpha t)^{-1/2}z] - C_2[(2\pi\alpha t)^{-1/2}z]\right] + \frac{1}{2}\sqrt{\frac{t}{\pi\alpha}}\sin\left(\frac{z^2}{4\alpha t} + \frac{\pi}{4}\right), \tag{43}$$

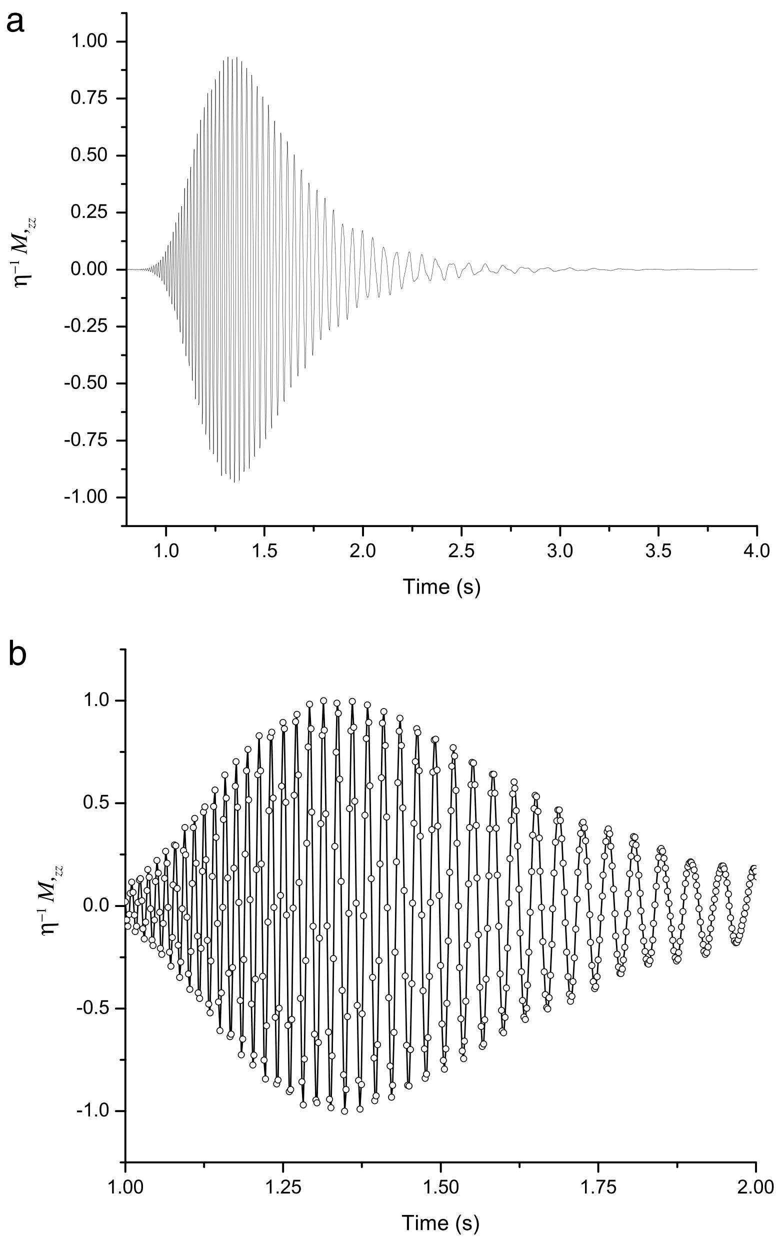

Fig. 9. Test of the reciprocity principle for the configuration shown in Fig. 5. Panel (a) shows experiments *A* and *B* (superimposed and normalized) corresponding to the first choice of sources in Eq. (37). A detail is shown in (b), where the solid line and empty dots correspond to experiments *A* and *B*, respectively.

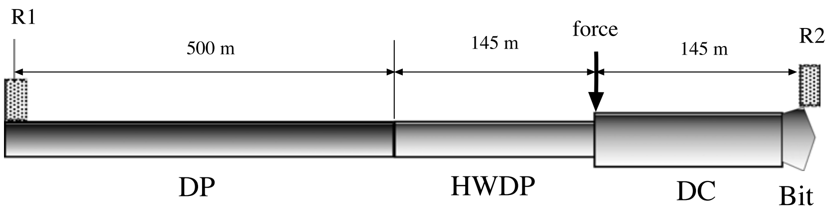

Fig. 10. Drill string with drill bit. The location of the deflection force f and of two receivers (R1 and R2) are indicated.

where

$$\alpha^2 = \frac{YI}{\rho A} = -\frac{\gamma}{\eta}, \tag{44}$$

and

$$C_2(x) = \frac{1}{\sqrt{2\pi}} \int_0^x \frac{\cos u}{\sqrt{u}} du \quad \text{and} \quad S_2(x) = \frac{1}{\sqrt{2\pi}} \int_0^x \frac{\sin u}{\sqrt{u}} du \quad \text{and} \tag{45}$$

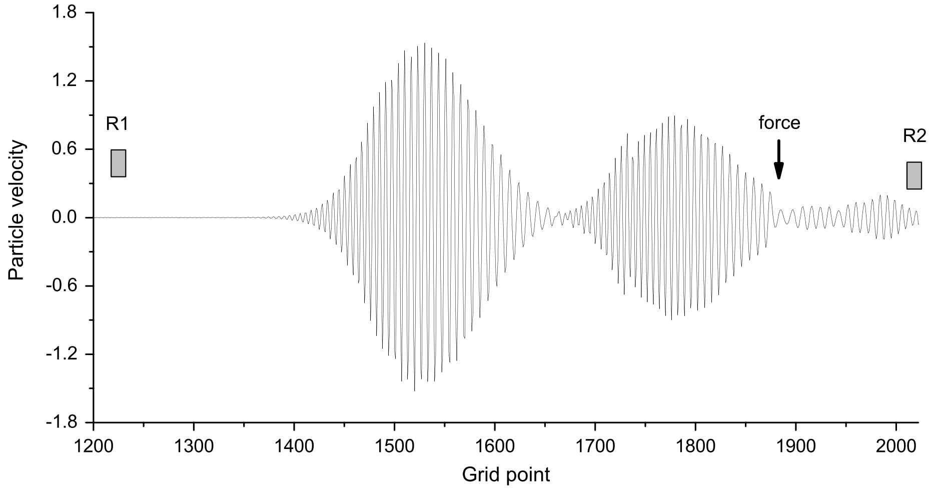

Fig. 11. Snapshot of the particle velocity at 1 s propagation, corresponding to the experiment shown in Fig. 10.

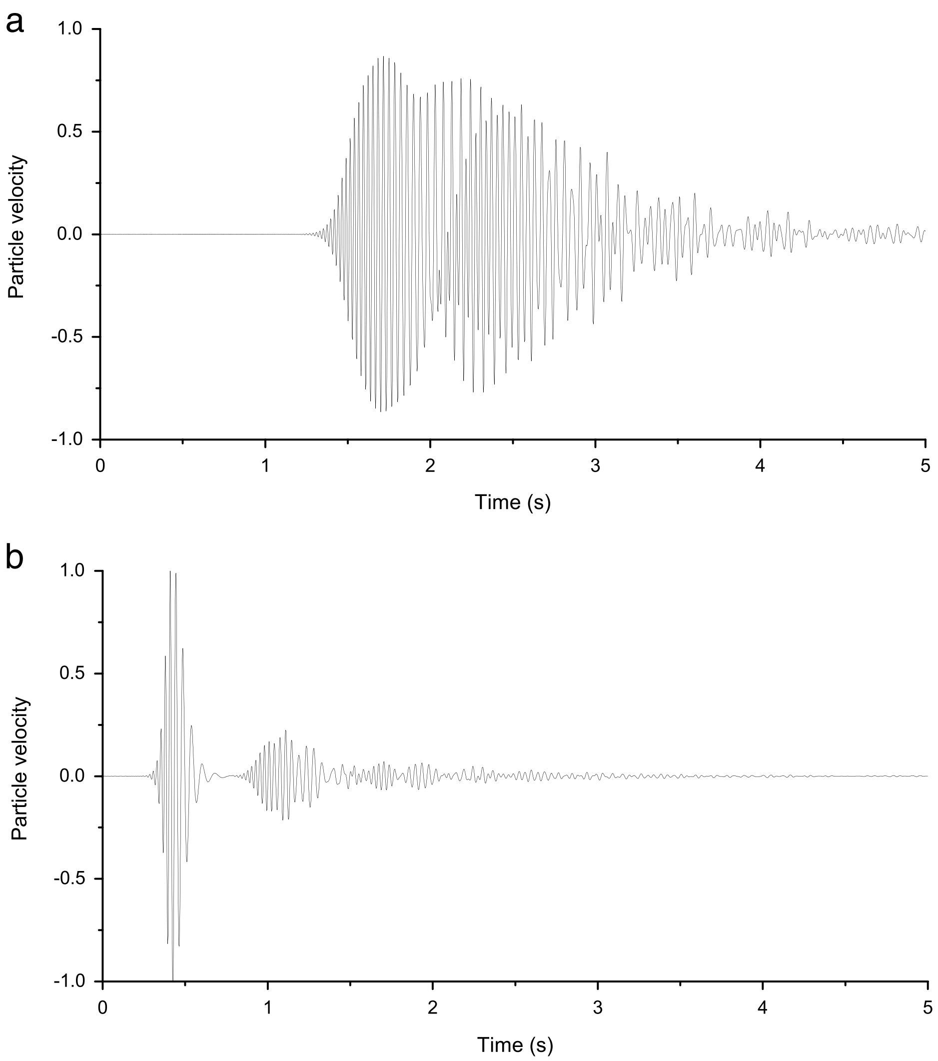

Fig. 12. Particle velocity at receivers R1 (a) and R2 (b) corresponding to the experiment shown in Fig. 10.

are Fresnel integrals [4]. The particle velocity is obtained as

$$v = G * \dot{h}, \tag{46}$$

where h is the time history (42) and "$*$" denotes time convolution. All these calculations are performed by discretizing the time variable.

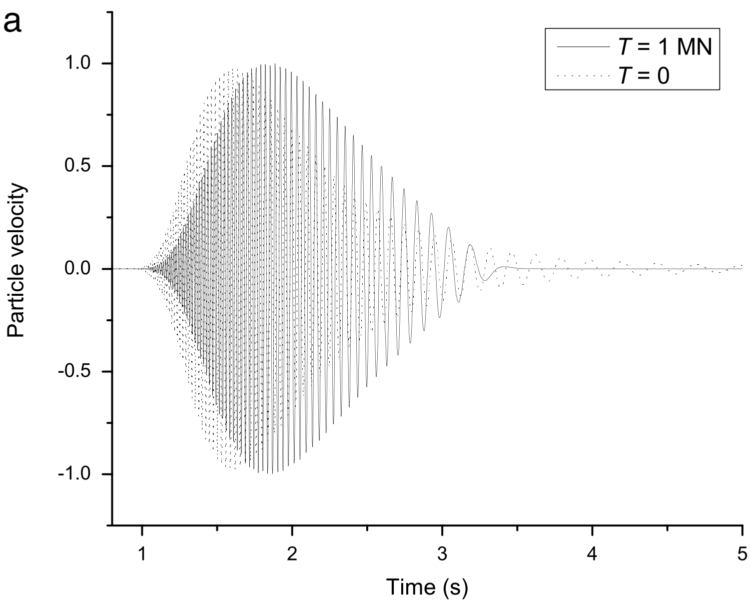

Fig. 13. Comparison between time histories with and without axial load. In (a) a constant load is applied to a drill pipe section (the source–receiver distance is 645 m), while (b) corresponds to experiment *A* of Fig. 4.

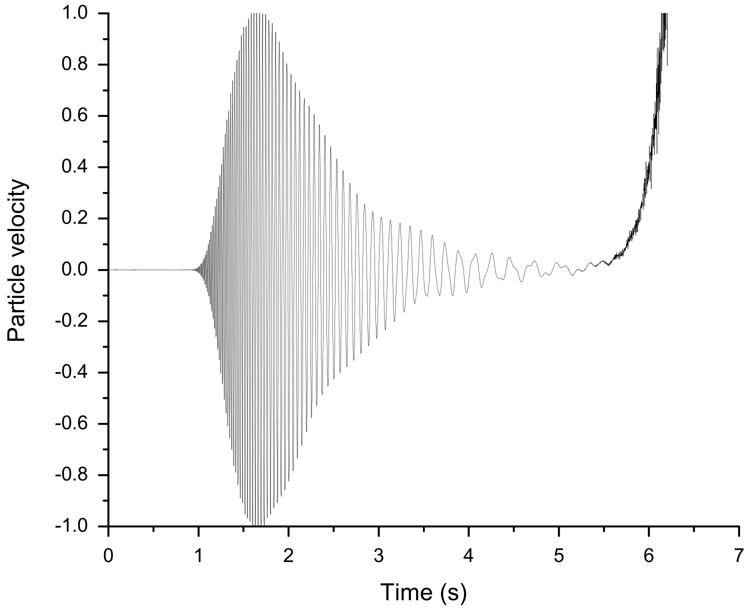

Fig. 14. Particle velocity corresponding to experiment *A* in Fig. 4, where part of the DC has a compressive load.

Eq. (46) corresponds to a solution of Eq. (1) with the force

$$s(t,z) = \delta(z)h(t), \tag{47}$$

where $v = \dot{w}$.

Since the bending moment satisfies $\dot{M} = \gamma v_{,zz}$ from Eq. (1), a solution from the Green function can be obtained as $M = \gamma(G * h)_{,zz}$.

References

[1] R.F. Mitchell, M.B. Allen, Lateral vibration: the key to BHA failure analysis, World Oil 400 (1985) 101–104.
[2] T.H. Hill, P.V. Seshadri, K.S. Durham, A unified approach to drillstem-failure prevention, SPE Drill. Eng. 7 (1992) 254–260.
[3] F. Poletto, F. Miranda, Seismic While Drilling—Fundamentals of Drill Bit Seismic for Exploration, Elsevier Science, 2004.
[4] K.F. Graff, Wave Motion in Elastic Solids, Dover Publications, Inc., 1975.
[5] W.C. Chin, Wave Propagation in Petroleum Engineering, Gulf Publishing Company, 1994.
[6] H. Hakimi, S. Moradi, Drillstring vibration analysis using differential quadrature method, J. Pet. Sci. Eng. 70 (2009) 235–242.
[7] J.D. Achenbach, Reciprocity in Elastodynamics, Cambridge University Press, 2003.

[8] J. Zare, S.J. Hashemi, R. Gholamreza, Finite element analysis of drillstring lateral vibration, J. Eng. Appl. Sci. 6 (2011) 64–70.
[9] R.-J. Shyu, Bending vibration of rotating drill strings, Ph.D. Thesis, MIT, 1989.
[10] V.I. Gulyaev, P.Z. Lugovoi, S.N. Khudolii, L.V. Glovach, Theoretical identification of forces resisting longitudinal movement of drillstrings in curved wells, Internat. Appl. Mech. 43 (2007) 1248–1255.
[11] S.M. Sahebkar, M.R. Ghazavi, S.E. Khadem, M.H. Ghayesh, Nonlinear vibration analysis of an axially moving drillstring system with time dependent axial load and axial velocity in inclined well, Mech. Mach. Theory 46 (2011) 743–760.
[12] J.M. Carcione, F. Poletto, Simulation of stress waves in attenuating drill strings, including piezoelectric sources and sensors, J. Acoust. Soc. Am. 108 (2000) 53–64.
[13] J.M. Carcione, Wave Fields in Real Media. Theory and Numerical Simulation of Wave Propagation in Anisotropic, Anelastic, Porous and Electromagnetic Media, second ed., revised and extended, Elsevier Science, 2007.
[14] J.E. White, Seismic Waves: Radiation, Transmission, and Attenuation, McGraw-Hill Book Company, 1965.
[15] R.D. Blandford, K.S. Thorne, Application of Classical Physics, California Institute of Technology, 2003.
[16] J.M. Carcione, F. Poletto, Electric drill-string telemetry, J. Comput. Phys. 186 (2003) 596–609.